ILASS 2008
Sep. 8-10, 2008, Como Lake, Italy

Paper ID ILASS08-2-17

EXPERIMENTAL AND NUMERICAL INVESTIGATION OF A MONOCOMPONENT POLYDISPERSE SPRAY

V. Bodoc*, J. Wilms*, Y. Biscos*, G. Lavergne*, O. Rouzaud*

*ONERA/DMAE, 2, av. Eduard Belin, BP 4025, 31055 Toulouse Cedex 4, France
Virginel.Bodoc@onecert.fr

ABSTRACT

In the objective of reduction of pollutant emission and identification of alternatives fuels, it is of great interest to improve the knowledge on mechanisms like droplet evaporation, heat transfer and droplet coalescence inside a fuel spray.

In a spray, the droplet evaporation rate is piloted by the physical properties of the liquid, the heat exchange with the environment and the droplet concentration. This paper presents an experimental and numerical study of an evaporating spray.

Different optical non-intrusive techniques were developed in order to measure parameters as the temperature and the size distribution of the disperse phase inside a cloud of droplets. Experimental tests are carried out on a polydisperse monocomponent droplets spray using Global Rainbow Refractometry technique. The measurement technique is described and the results are presented for different liquids, injection temperatures and positions in the spray.

In the second part of this paper two-dimensional Reynolds-Averaged Navier-Stokes (RANS) simulations are carried out using the CEDRE code developed at ONERA. The discrete phase is solved by an Lagrangian approach. The numerical results are compared to the experimental ones in order to validate the evaporation models in the case of monocomponent droplet sprays.

INTRODUCTION

Sprays play an important role in a wide area of industrial and agricultural applications: aeronautics, automotive industry, chemical industry, cosmetics, pesticide dispersion.

Droplet behaviour inside a spray is strongly dependent of the spray characteristics. The spray dynamics and the evaporation rate are very dependent of the volume fraction of the dispersed phase.

For the validation of the evaporation models in such configurations, it is necessary to measure the local droplet size, velocity ant temperature.

There are two main objectives of this paper. For the experimental part, we are interested in the spray investigation by the use of Particle Doppler Anemometry (PDA) and Global Rainbow Refractometry (GRR) techniques. If the firs one is largely used for droplets size and velocity measurement since many years, the second one is still under development. As liquids the n-hexadecane and n-octane are used.

In the second part of this paper, a numerical simulation tool is developed in order to validate the evaporation models in the case of a spray generated in a non-confined configuration and in a stagnant air.

Global Rainbow Refractometry

Even though the Rainbow Refractometry is used for almost 20 years, its applicability was limited to mono-disperse sprays.

It is well known that, when a droplet cross a laser beam the rainbow phenomenon occur. If a spherical shape droplet is assumed, the rainbow optical signal gives both temperature and diameter. Nevertheless, the droplet non- sphericity and the temperature gradient inside the droplet strongly modify rainbow optical signal.

The basic principle of the GRR technique is the summation of these rainbows signals corresponding to the droplets of different shapes, dimensions and temperatures. The pattern is formed by constructive interference of laser light scattered by the spherical droplets of different sizes. As in the case of natural rainbow, the non-sphericity effect is eliminated by destructive interference yielding an uniform background.

Several studies using the Airy theory to estimate the scattered light intensity in function of the droplet diameter and temperature were developed. With an inversion method the droplets refractive index at the different positions in the spray is measured. Van Beek and all [1] proposed several inversion algorithms of the global rainbow optical signal based on the Airy theory and on the assumption that the size distribution is log-normal function. Different data inversion algorithms are proposed but the most interesting results are obtained from the one based on the inflexion point around the main rainbow maxima. This technique was applied afterwards in different configurations investigations [2,3] proving its large applicability.

Later, S. Saengkaew and all [4], using empirical correction coefficients, found that Complex Angular Momentum Theory (CAM) developed by Nussenzveig can be applied within an angular range, wider than for the Airy theory. Moreover, the scattered light can be provided successfully in a large range of refractive indices and particle sizes. More specifically, it was demonstrated that the modified Nussenzveig theory furnishes predictions of rainbow refractive intensities close to Lorentz –Mie theory but it requires a very reduced computation times, similar to the computation times in Airy approach.

The GRR technique proved afterwards its capacity in radial gradient temperature investigation [5,6].

EXPERIMENTAL INVESTIGATION OF THE SPRAY

Experimental setup.

The experimental setup used in this study is the same as in the references [7,8], where it is more detailed**.**

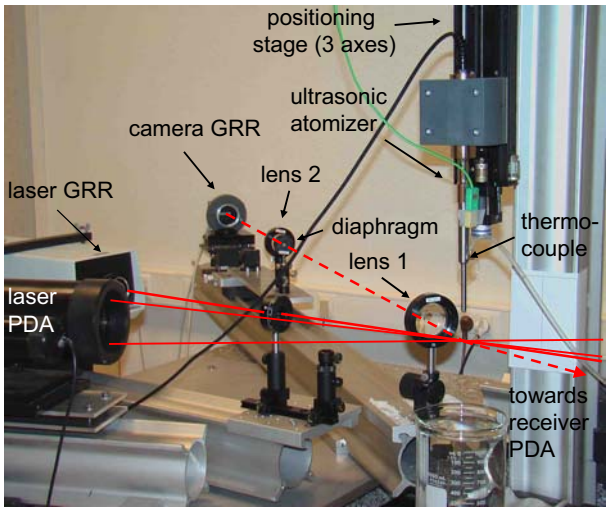

Figure 1. Photograph of the setup

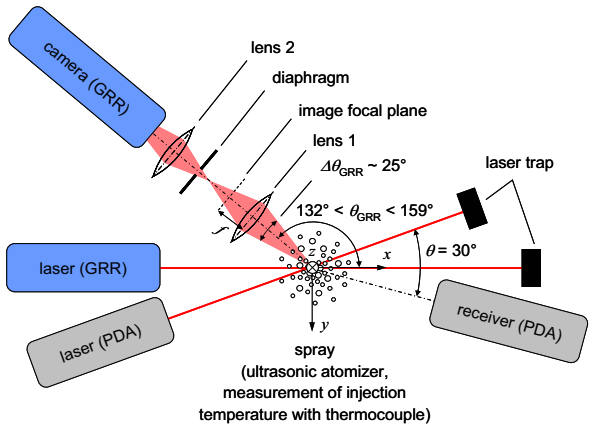

Figure 2. Schematic top view of the setup

The spray generator is an ultrasonic atomizer Sonics (USVC130 AT), 20 kHz (Fig.1). The size distribution and the spray geometry are controlled by the amplitude of the generator excitation and by the liquid flow rate. The liquid temperature is controlled with a thermostat. The atomizer is fixed onto a system with three degree of freedom. The vertical displacement is piloted by the computer.

For the GRR technique a HeNe continue laser, delivering a power of 30 mW is used. In the Fig.2 the optical reception system is detailed. The first lens realises a Fourier transformation of the optical signal. In this way, the scattered light intensity is expressed only in function of the angle and is independent of the droplet position in the measure volume. The image of the optical Fourier transformation is reproduced by the second lens on the camera CCD linear sensor. A diaphragm disposed before the second lens let the possibility to control the measurement volume.

All the optical arrangement can be rotated in order to permit the measurement in the backward side of an angle from 132 to 151°. The optical system allows acquisition of light intensity scattered in an angular window of about 25° for 2048 pixels of the CCD sensor. This optical system offer the possibility of refractive index measurement between 1,25 – 1,45.

The PDA receiver is disposed in forward diffusion at 30° angular position. The scattered light at this position is dominated by the first order refraction for a parallel polarisation. This angle can be used for a large interval of refractive index (1.03<n<2) allowing the measurement for many liquids.

CCD linear camera calibration.

The CCD sensor used for GRR technique is made by 2048 pixels. In order to obtain a relation between the pixel number and the angular position a calibration is done by the use of a laser beam reflected by a mirror. The mirror is disposed on a micrometric rotating plate with 0,001° resolution. The reference angular position is done by the superposition of incident and reflected laser beams. Afterwards for different angular positions the lighted pixel number is recorded. A 3 order polynomial correlation is used. The error of this correlation is ±0.001°.

The refractive index - temperature correlation.

The GRR technique provides the refractive index of the droplets. The correlation between the refractive index and the liquid temperature need to be known to determinate the average temperature of the droplets. For some liquids the literature gives such correlations. Nevertheless we can check theses results by using a multi spectral refractometer available in our laboratory.

For n-hexadecane and n-octane we used a 632,8 nm wavelength laser to measure the refractive index as a function of temperature. The results show a linear evolution of these two parameters.

Inversion technique.

From the global rainbow optical signal, the droplets temperature is determined by using an inversion code developed at the CORIA par S. Saengkaew and G. Gréhan [9]. By the use of the non-negative least square method (nnls) with light intensity computed by Nussenzveig theory and minimizing the distance between the recorded and computed global rainbow pattern, a mean refractive index and a size distribution are extracted. Although this algorithm gives also the droplet size distribution in the spray, we observe that the results are strongly depending on the code input parameters values: number of classes, number of computing points, minima and maxima angles. For this reason, the code is used only for the temperature measurement.

Monocomponent polydisperse spray investigation.

For all our measurements a flow rate of 35 ml/min and disintegration amplitude of 30 % were used. The incident laser beam absorption is supposed to be too weak to influence the spray temperature or droplets evaporation.

A first feasibility study was investigated by using n-hexadecane (T_b=286 C) which has a very low evaporation rate in order to avoid the thermal gradient in the droplet. The liquid was injected at the ambient temperature (T_{amb}~26 C).

If the liquid and the air temperatures are equal, the spray temperature is constant and this parameter was recorded by the thermocouple disposed inside the atomizer.

Measurements are performed in XZ plane in different location in the spray (Fig. 3). The grid was chosen refined enough to build a very detailed data base to be used for the validation of other numerical approaches and to be available for another research works in the future.

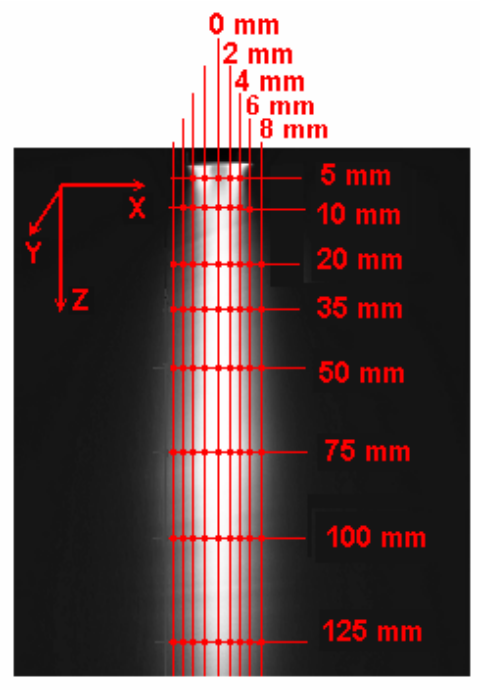

Figure 3. Measurements locations in the spray

The radial temperature evolutions, for three different distances from the nozzle, are plotted in Fig.4.

The discrepancy between the GRR results and the thermocouple values is low, about 1 C. This can be explained by the effect of the very low droplet evaporation due to the convection effect (relative velocity ~1 m/s) and by the accuracy of the technique.

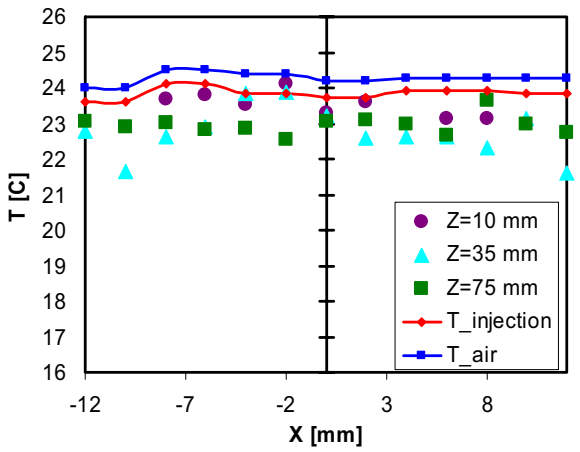

Figure 4. Radial evolution of the temperature for the n-hexadecane.

Further on the n-octane is used in reason of a more volatility and results will be compared with the numerical results.

NUMERICAL SIMULATION OF THE SPAY.

Numerical simulation of the spray is carried out using the code CEDRE developed at ONERA. This code provides multiple modules making-it useful in the multiphase flow investigation.

A two-way coupling treatment of the spray dynamics is realised through an Eulerian-Lagrangian stochastic approach. The main advantage of a Lagrangian tracking technique is that it allows a detailed study of the droplets.

The unsteady technique used in this numerical computation consists in the following of a large number of numerical droplets representing real droplets with closes properties: position, radius, velocity, temperature.

Computing domain and boundary conditions

The configuration of the experimental setup has been presented in the previous chapter. This configuration is considered axisymmetric for the computation. The spray is generated at the section orifice in the computing domain of 0.15 x 0.2 m^2. The injection is directed downward in this symmetrical configuration.

The experimental results showing a quasi-symmetrical evolution of the spray pattern, a bi-dimensional configuration has been chosen for the computation. This approach allows us moreover to reduce the computational cost. A large number of cells is required in the vicinity of the atomizer surface, due to the high droplet concentration.

The choice of the boundary conditions was made taking into account the CEDRE available models suited to the physical phenomenon. As the computation is performed for two phases, boundary conditions need to be provided for both of them. In the Fig. 5 all the boundary conditions are presented. We note that italic capital letters are used to denote the discrete phase's boundary conditions.

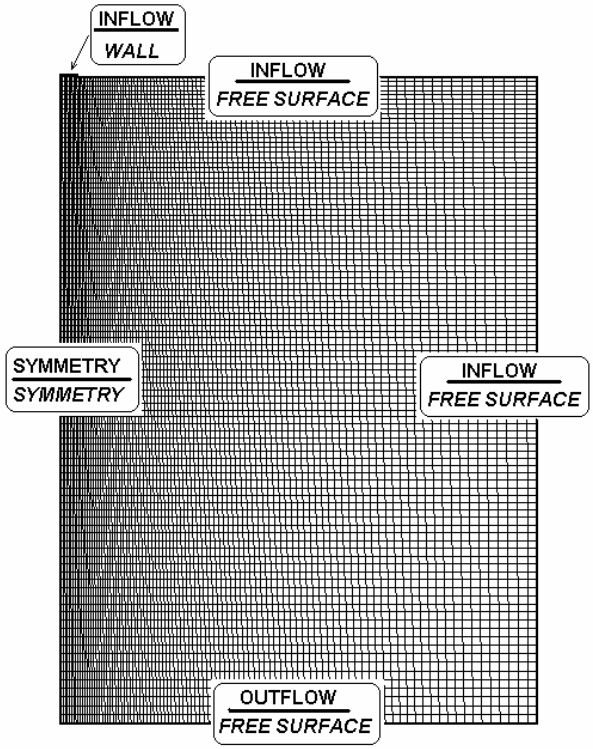

Figure 5. The computing domain geometry and boundary conditions

For the continuous phase, an Inflow type condition is used for the most of the boundaries. Thus an subsonic flow is assumed and parameters like pressure, temperature, turbulent kinetic energy and the turbulent dissipation rate need to be provided. The values of the turbulent kinetic energy and the turbulent dissipation were estimated supposing that the turbulent intensity is about 10%. This values are not simple to introduce and could affect the spray dynamics unless a very large computational domain is considered with penalties for the computing time.

As for discrete phase all the boundary conditions are supposed to be of the *free surface* type, except the one corresponding to the atomizer surface. In this case a *wall* type without droplet deposition is imposed. During the numerical processing all the droplets are followed till they reach the limits of the computational domain. After that they are considered as escaped and no other influence is considered as rebound, splash or deposition.

Initial conditions

The unsteady numerical simulation of a Lagrangian spray emerging in a free atmosphere is difficult to be realized especially in the first phase, that corresponds to the transition from the t=0 s to the stable state. During this time period the continuous phase is accelerated as a consequence of the droplets injected with a high velocity. To pass over this problem we impose a low velocity as initial condition for the continuous phase.

As for the discrete phase there are no droplets in the computing domain at the initial moment.

Simulation of the gas phase

A Navier-Stokes model is used in order to simulate the continuous phase behavior. The turbulent effects were taken into account by the mean of a *RANS* model. The *k-ε* turbulence model was selected as a consequence of its applicability to a large domain of aerodynamic phenomena.

Simulation of the dispersed phase

Lagrangian stochastic particle model is based on the statistical approach of the randomly modelled droplets trajectories.

The tracking of the droplets injected in the air is done taking into account gravity, drag, heating, vaporisation and turbulent dispersion.

The following system of equations characterize each droplet:

$$dx_p = v_p \cdot dt \qquad \textbf{(1)}$$

$$dv_p = \frac{U_g + u_p - v_p}{\tau_p} \cdot dt + g \cdot dt \qquad \textbf{(2)}$$

$$du_p = -\frac{u_p}{\tau_{gp}} \cdot dt + \sqrt{\frac{4 \cdot k_g}{3 \cdot \tau_{gp}}} \cdot dW_t \qquad \textbf{(3)}$$

$$\frac{d(r_p)^2}{dt} = -\frac{\mu_g \cdot Sh}{\rho_p \cdot Sc} \cdot \ln(1 + B_M) \qquad \textbf{(4)}$$

$$m_p c_{pl} \frac{dT_p}{dt} = 2\pi \cdot Nu \cdot \lambda_g \cdot r_p \cdot (T_g - T_p) \cdot \frac{\ln(1 + B_T)}{B_T} - \frac{dm_p}{dt} \cdot L_v(T_p) \qquad \textbf{(5)}$$

In the Eq (2) the gravity effects are considered and by the means of the dynamic relaxation time τ_p expressed in the Eq (6) the drag force is taken into account.

$$\tau_p = \frac{8 \cdot \rho_p(T_p) \cdot r_p}{3 \cdot C_D \cdot \rho_g \cdot \|U_g + u_p - v_p\|} \qquad \textbf{(6)}$$

The Shiller & Neuman correlation is used in order to relate the droplet drag coefficient to the droplet vaporisation (Eq. (7)).

$$Cd = \begin{cases} \frac{24}{\mathrm{Re}_p} \cdot (1 + 0.15 \cdot \mathrm{Re}_p^{0.687}) & if\ \mathrm{Re}_p \le 1000 \\ 0.445 & if\ \mathrm{Re}_p \ge 1000 \end{cases} \qquad \textbf{(7)}$$

where $\mathrm{Re}_p = \frac{2 \cdot \rho_g \cdot \|U_g + u_p - v_p\| \cdot r_p}{\mu_g}$ stands for the particle Reynolds number.

Equation (3) yields the Langevin stochastic differential equation witch is modelling the particle turbulent diffusion. In this equation the τ_{gp} represents the turbulent autocorrelation time scale along the streamline and is expressed as

$$\tau_{gp}^3 = \frac{\tau_a}{\sqrt{1 + \frac{1}{2} \cdot \left(\frac{\tau_a}{\tau_b}\right)^2}}, \text{ where:}$$

$$\begin{cases} \tau_a = \frac{l_g}{\sqrt{\frac{2}{3} \cdot k_g}}, \\ \tau_b = \frac{l_g}{\|U_g + u_p - v_p\|} \end{cases} \text{ and the lagrangian integral scale is:}$$

$$l_g = 0.09^{3/4} \cdot \frac{k_g^{3/2}}{\varepsilon_g}$$

As evaporation modifies droplet size, Eq. (4) is used to predict droplet diameter decrease. Convection influence on the evaporation rate is taken into account by the use of the Ranz-Marshall model for the Sherwood number as in Eq. (8).

$$Sh = 2 + 0.57 \cdot \mathrm{Re}^{1/2} \cdot Sc^{1/3} \qquad \textbf{(8)}$$

The temperature evolution is evaluated using Eq. (5). The droplet cooling is calculated with the Ranz-Marshall assumption for the Nusselt number as in Eq (9).

$$Nu = 2 + 0.57 \cdot \mathrm{Re}^{1/2} \cdot \mathrm{Pr}^{1/3} \qquad \textbf{(9)}$$

Average thermophysical properties near the droplet surface are obtained with the 1/3 rule.

Note that phenomenon like secondary break-up, collisions and coalescence are neglected. As the liquid volume fraction varies from $7 \cdot 10^{-4}$ to $2 \cdot 10^{-3}$ inside the spray (PDPA results) this assumption seems to be correct.

Injection modelling.

A special attention we devoted to the droplets injection.

The Lagrangian approach used in this simulation is very attractive for predicting spray dispersion, heat and mass transfer. However this approach needs as input the initial droplet size and velocity distributions.

The size and velocity distributions as well as the temperature were measured at 5 mm from the atomizer surface.

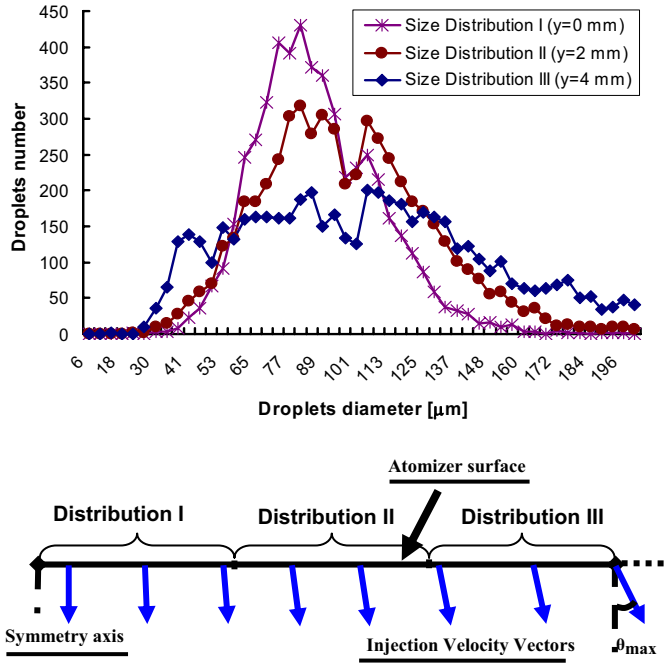

Figure 6. Injection modelling

As we presented in the Fig.3 several radial measurements are available. Size distribution shape changes with the position of the measurement volume within the spray (Fig. 6). This heterogeneity in size distribution is taken into account as it is presented in the down side of the Fig. 6. Every size distribution is supposed to be characteristic to a limited interval of the injector surface. Moreover, as it is almost impossible to use the real distributions furnished by the PDA in the reason of the great number of classes we propose to employ a simplified distribution. Thus only 5 classes are used and the average technique is explained throughout the Fig. 7.

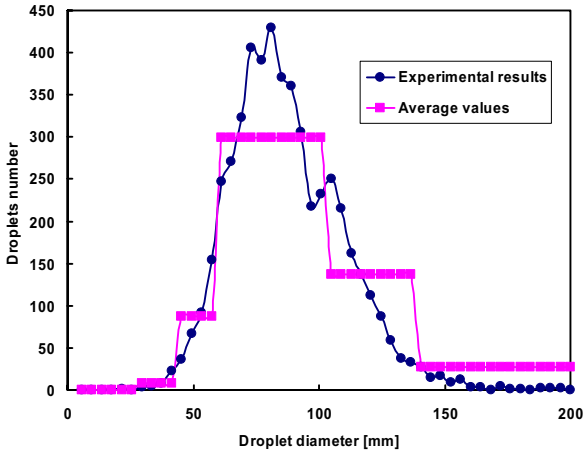

Figure 7. Droplet size distribution modelling

For every distribution and class the mean number of droplets is calculated with the Eq. (10):

$$N_{c,d} = \frac{\sum_{i=1}^{n_{c,d}} N_i}{n_{c,d}}, \; c = \overline{1,5} \;, \; d = \overline{1,3} \qquad \textbf{(10)}$$

Injected droplets diameter is calculated with Eq (11):

$$D_{c,d} = \frac{\sum_{i=1}^{n_{c,d}} n_i \cdot D_i}{\sum_{i=1}^{n_{c,d}} n_i}, \; c = \overline{1,5} \;, \; d = \overline{1,3} \qquad \textbf{(11)}$$

As for the velocity it was balanced with the droplet diameter as in Eq.(11) and thus for every class and distribution, the droplets injection velocity is constant.

$$V_{cd} = \frac{\sum_{i=1}^{n_{cd}} V_i \cdot n_i \cdot D_i^3 \cdot}{\sum_{i=1}^{n_{cd}} n_i \cdot D_i^3} \qquad \textbf{(12)}$$

As for the injection points positioning, the injection surface is divided in 25 intervals so that for every class and interval corresponds an injection point. The position of this point was determined randomly.

Based on these assumptions a small Fortran code is realized and used to generate an injection file that provide CEDRE with all information related to the droplets.

RESULTS

Fig. 8 is a representation both of the droplets and the gas phase after the spray gets a stable state. Left-side figure presents typical behaviour of droplets as a result of the Lagrangian computation. The geometry of the spray illustrates the same shape observed experimentally (Fig. 3).

The large droplets are affected only by their injection angles, velocity and gravity whereas small droplets trajectories are governed rather by the gas phase. This phenomenon is explained, throughout the Stokes number, by the differences between the characteristic times of the two phases. Because of their low inertia, droplets of the most reduced diameter are following the continuous phase

streamlines. As indicated in the right-side of the Fig. 8, falling droplets are creating an absorption of the air, streamlines being almost perpendicular to the spray pattern.

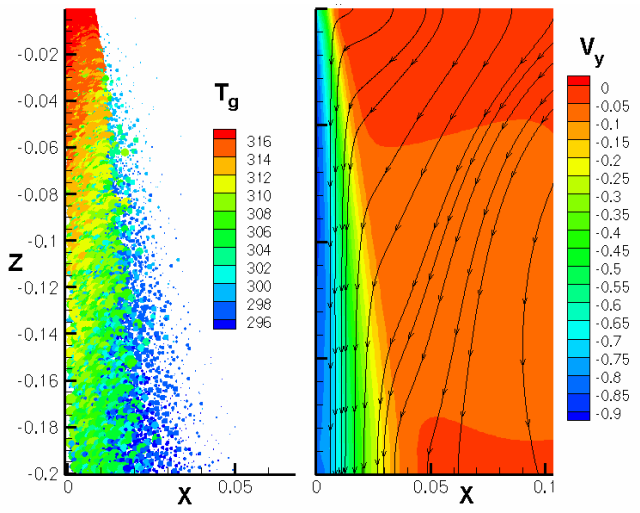

Figure 8. Left-hand side: droplet distribution in the spray. Right-hand side: continuous phase velocity

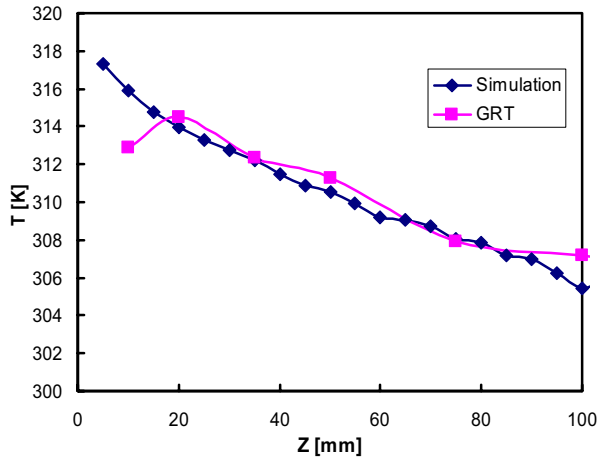

Figure 9. Longitudinal evolution of the droplet temperature (X=0 mm)

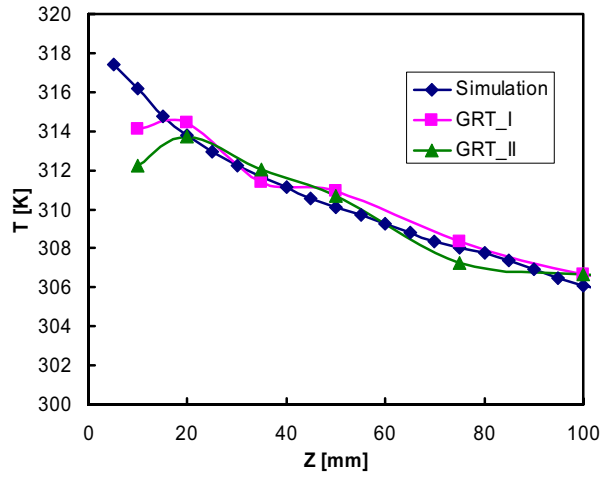

Figure 10. Longitudinal evolution of the droplet temperature (X=2 mm)

For the comparison with experimental data, we are interested in useful results, namely the temperature, velocity and droplet size as a function of the position in the spray.

Fig. 9 and Fig.10. present the axial evolution of the droplets temperature. As experimental measurements were realised symmetrically in respect to the spray axis the two evolutions were represented on the same side of the Z-axis. Numerical and experimental results are in good agreement except in the near injector area. It seems that at Z=5 mm and Z=10 mm the temperature values furnished by GRR technique are non-realistic as these values are significantly inferior to the liquid temperature. (We remember that the liquid temperature is well measured at the injector nozzle by the thermocouple). Actually, during the experimental measurement campaign we realized that it is very difficult to have a realistic temperature under 20 mm from the spray nozzle. On the one hand the high density of the dispersed phase suppress the Global Rainbow optical signal by multiple scattering. On the other hand the quality of the optical signal is altered by the non-spherical shape of the droplets present in this region of the spray.

In order to run over this problem, in the numerical simulation the temperature of the injected droplets was estimated by the extrapolation of the values measured downstream in the spray (Fig. 9-10).

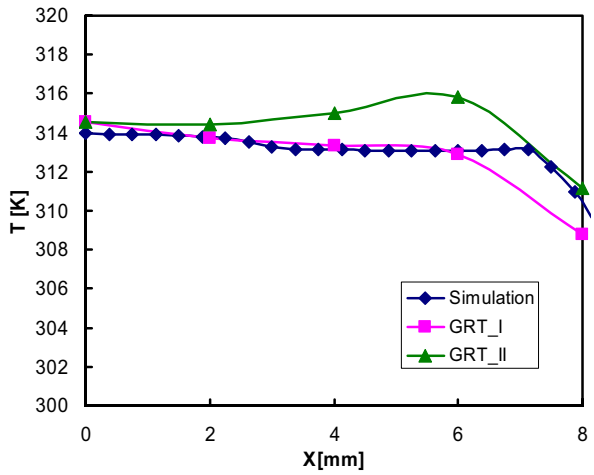

Figure 11. Radial evolution of the droplet temperature (Z=20 mm)

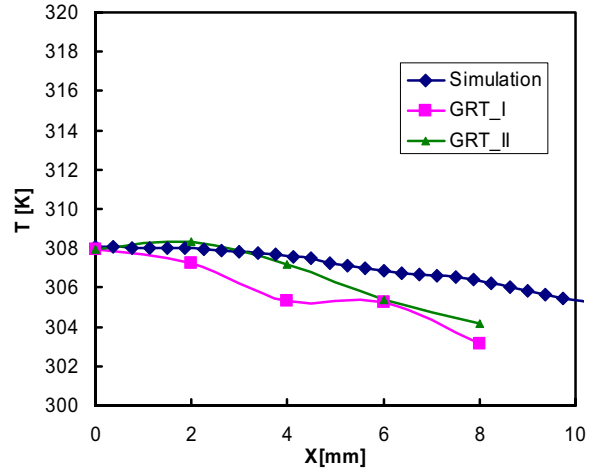

Figure 12. Radial evolution of the droplet temperature (Z=75 mm)

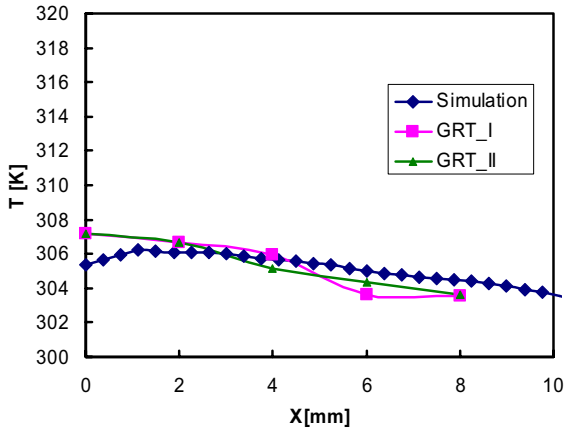

Figure 13. Radial evolution of the droplet temperature (Z=100 mm)

Radial evolutions of the droplets temperatures are also plotted for different distances from the atomizer (Fig.11-13). Generally, the differences between the experimental and numerical results are inferior to 2 K. The temperature decreases with the radius in reason of the higher thermal transfer between the two phases at the spray boundaries.

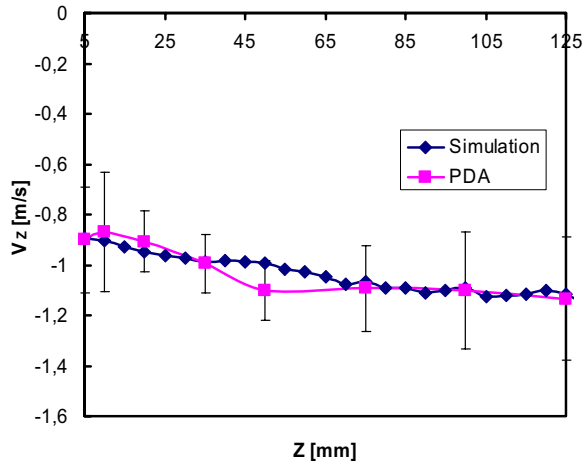

Figure 14. Longitudinal evolution of the droplets velocity (X=0 mm)

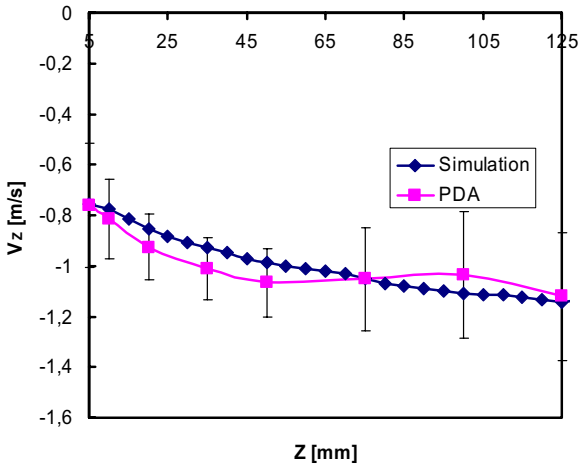

Figure 15. Longitudinal evolution of the droplets velocity (X=2 mm)

Concerning velocity and mean diameter we found the same tendency in their evolution, although there are local differences (Fig. 14-15).

Globally, large droplets are creating a core which is filled by small droplets leading to a heterogeneous droplet distribution. The heterogeneity in the droplet distribution can be illustrated computing the evolution of the mean diameter D10 as a function of both longitudinal and radial position. Fig. 16 presents the numerical results in comparison with the experimental ones. As it can be seen, the longitudinal evolution of the D10 is defined by an increase till a value of about 90 μm is reached. This evolution can be explained by the small droplets evaporation. Away from the injector surface the large droplets contribute more and more to the computation of the average size. As for radial evolution of the mean diameter, we can see (Fig. 17-18 that the numerical results are close to the experimental ones. If at 35 mm from the injector surface, the average diameter increases with the radius, at 100 mm downstream on the axis the spray seems to be more homogenous.

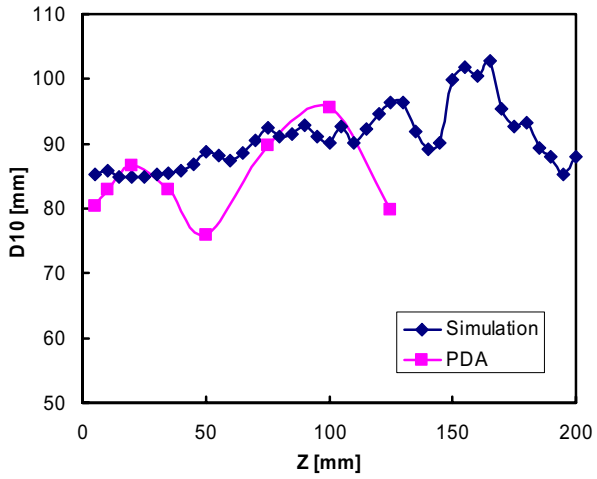

Figure 16. Longitudinal evolution of the mean diameter (X=0 mm)

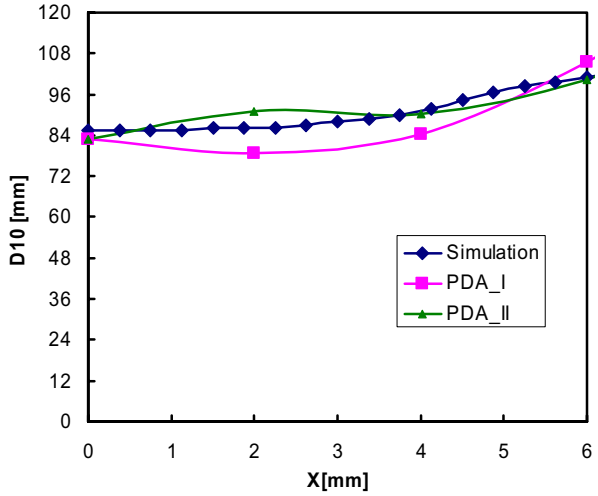

Figure 17. Radial evolution of the mean diameter (Z=35 mm)

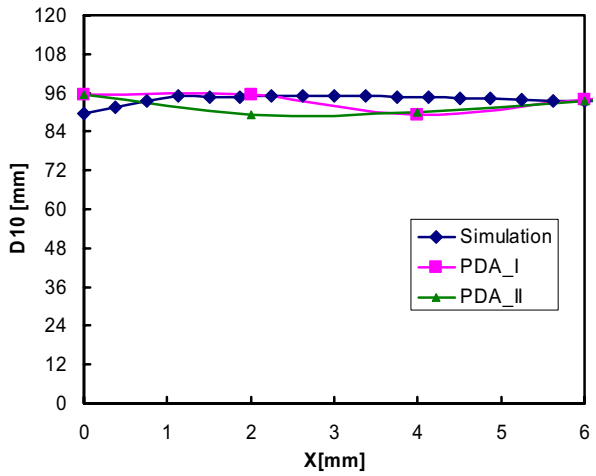

Figure 18. Radial evolution of the mean diameter (Z=100 mm)

CONCLUSIONS

The present work was carried out in order to under take a detailed simulation of a spray behavior using the droplets temperature, size and velocity distributions available at the well defined position in the spray. The spray is analyzed in a non-confined, stagnant environment.

In the first part of the paper we focused on the experimental setup and especially on the Global Rainbow Refractometry technique. A feasibility study was realized in the objective of this technique evaluation. A low rate evaporation liquid at the atmospheric temperature was used and the GRR results were compared with those recorded by a thermocouple. The well fitting of these results encouraged us in the use of GRR technique coupled with a PDA to realize systematic measurements of the droplets parameters inside the spray. A higher evaporating liquid was selected.

The new results were compared in the second part of the paper with the numerical ones. The numerical simulation was based on the heating and evaporation models already implemented in the CEDRE code. The quantitative agreement with the measure data proved that these models are able to be used in monocomponent liquid spray prediction

ACKNOWLEDGMENT

This research project has been supported by a Marie Curie Early Stage Research Training Fellowship of the European Community's Sixth Framework Programme under contract number MEST-CT-2005-020426.

NOMENCLATURE

Symbol	Quantity	SI Unit
V_{cd}	Class average velocity	m/s
k_g	Gas turbulent kinetic energy	m^2/s^2
ε_g	Gas dissipation rate	m^2/s^3
Re_p	Droplet Reynold number	
U_g	Gas mean velocity	m/s
u_p	Droplet fluctuating velocity	m/s
v_p	Droplet velocity	m/s
ρ_p	Droplet density	kg/m^3
ρ_g	Gas density	kg/m^3
μ_g	Gas dynamic viscosity	$Pa\ s$
r_p	Droplet radius	m
m_p	Droplet mass	kg
λ_g	Gas thermal conductivity	W/mK
c_{pl}	Specific heat capacity	$J/kg\ K$
T_g	Gas temperature	K
T_p	Droplet temperature	K
l_g	Turbulent integral scale	m
τ_p	Dynamic relaxation time	s
τ_{gp}	Turbulence autocorrelation time	s
C_D	Drag coefficient	
W_t	Wienner process	
Nu	Nusselt number	
Sh	Sherwood number	
B_M	Mass Spalding number	
B_T	Heat transfer Spalding number	
Pr	Gas Prandtl number	
c	Class number	
d	Distribution number	

REFERENCES

[1] J.P.A.J. van BEECK, L. Zimmer and M.L. Riethmuller, Global Rainbow Thermometry for Mean Temperature and Size Measurement of Spray Droplets, *Particle & Particle System Characterisation*, vol. 18, pp. 196-204, 2001

[2] P. Lemaitre and all, Développement de la réfractometrie arc-en-ciel global pour mesurer la température des gouttes en chute libre, *Proc. Symp. 9e Congrès Francophone de Vélocimétrie Laser*, pp. F.2.1-F.2.9, 2004

[3] D. Yildiz, J.P.A.J. van Beeck, M.L. Riethmuller, Global Rainbow Thermometry applied to a flashing two-phase R134-A Jet,

[4] S. Saengkaew and all., "Rainbow refractometry: On the validity domain of Airy's and Nussenzweig's theories," *Optics Communications*, vol 259, pp. 7-13, 2006

[5] M.R. Vetrano and all, Mesures de la température d'un spray d'eau chaude par la méthode globale par arc-en-ciel : effet du gradient de la température dans les gouttes, *Proc. Symp. 9e Congrès Francophone de Vélocimétrie Laser*, pp. F.3.1-F.3.8, 2004

[6] S. Saengkaew and all, Rainbow refractometry on particles with radial refractive index gradient, *Exp. Fluids*, vol 43, pp. 595-601, 2007

[7] J. Wilms, Y. Biscos, S. Saengkaew, G. Gréhan and G. Lavergne, Precision and Applicability of Global Rainbow Refractometry for Measurements in Sprays, *Optics Communications* , 2007

[8] J. Wilms, G. Gréhan and G. Lavergne, Global Rainbow Refractometry with Selective Imaging Method, *Part. Part. Syst. Charact.*, vol 25, pp. 39-48, march 2008

[9] S. Saengkaew, Study of spray heat up: On the development of global rainbow techniques, Ph.D. thesis, Rouen University, 2005